Aalborg Universitet

AALBORG UNIVERSITY
DENMARK

Transferring the Incremental Capacity Analysis to Lithium-Sulfur Batteries

Knap, Vaclav; Kalogiannis, Theodoros; Purkayastha, Rajlakshmi; Beczkowski, Szymon; Stroe, Daniel-Ioan; Schaltz, Erik; Teodorescu, Remus

Published in:
ECS Transactions

DOI (link to publication from Publisher):
10.1149/07711.1919ecst

Publication date:
2017

Document Version
Accepted author manuscript, peer reviewed version

Link to publication from Aalborg University

Citation for published version (APA):
Knap, V., Kalogiannis, T., Purkayastha, R., Beczkowski, S., Stroe, D-I., Schaltz, E., & Teodorescu, R. (2017). Transferring the Incremental Capacity Analysis to Lithium-Sulfur Batteries. *ECS Transactions*, *77*(11), 1919-1927. https://doi.org/10.1149/07711.1919ecst

General rights
Copyright and moral rights for the publications made accessible in the public portal are retained by the authors and/or other copyright owners and it is a condition of accessing publications that users recognise and abide by the legal requirements associated with these rights.

- Users may download and print one copy of any publication from the public portal for the purpose of private study or research.
- You may not further distribute the material or use it for any profit-making activity or commercial gain
- You may freely distribute the URL identifying the publication in the public portal -

Take down policy
If you believe that this document breaches copyright please contact us at vbn@aub.aau.dk providing details, and we will remove access to the work immediately and investigate your claim.

Downloaded from vbn.aau.dk on: September 21, 2023

Transferring the Incremental Capacity Analysis to Lithium-Sulfur Batteries

V. Knap[a], T. Kalogiannis[a], R. Purkayastha[b], S. Bęczkowski[a], D.-I. Stroe[a], E. Schaltz[a] and R. Teodorescu[a]

[a] Department of Energy Technology, Aalborg University, Aalborg, 9000, Denmark
[b] Oxis Energy Ltd, Culham Science Centre, Abingdon, Oxfordshire OX14 3DB, United Kingdom

In order to investigate the battery degradation and to estimate their health, various techniques can be applied. One of them, which is widely used for Lithium-ion batteries, is the incremental capacity analysis (ICA). In this work, we apply the ICA to Lithium-Sulfur batteries, which differ in many aspects from Lithium-ion batteries and possess unique behavior. One of the challenges of applying the ICA to Lithium-Sulfur batteries is the representation of the IC curves, as their voltage profiles are often non-monotonic, resulting in more complex IC curves. The ICA is at first applied to charge and discharge processes at various temperature levels and afterward the technique is applied to a cell undergoing cycling degradation. It is shown that the ageing processes are trackable from the IC curves and it opens a possibility for their utilization for state-of-health estimation.

Introduction

With a growing number of battery applications in today's world, there is a lot of interest into methods of detecting, estimating, and analyzing battery degradation. Consequently, many different health detection and estimation methods and techniques have been proposed. Among these is the incremental capacity analysis (ICA) (1) method, which has generated significant interest in the Lithium-ion (Li-ion) batteries research and development. The method offers the possibility to analyze the ageing processes (e.g. loss of lithium inventory, loss of active material and kinetic changes) of Li-ion batteries and also has the potential to be implemented into a battery management system (2).

Dubarry et al. in (1) characterized ICA as a method which can track the electrochemical properties of a cell during a charge or discharge. These properties that are associated with the intercalations and the phase transformations can be seen at the voltage curves as the steep increases or the plateau regimes and they are translated into identifiable dQ/dV peaks when differentiating the capacity over the voltage. Several studies have been made for different Li-ion chemistries, different C-rates and temperatures as well as aging conditions. Specifically, Kassem et al. (3) stored LFP/G cells at different temperatures and SOC levels. The capacity fade under the different calendar conditions was investigated and the corresponding IC peaks for the different cases were compared. A reverse proportional trend of the IC peak to the temperature and SOC storage levels was observed. Dubarry et al. (4) investigated the IC behavior and identified the possible aging mechanisms of two different designed $LiFePO_4$ – based, 10

Ah Li-ion cells, a prismatic and a cylindrical, for cycle aging and at two different temperatures. Also in (5), Dubarry et al. examined the degradation of ten 1.9 Ah commercial 18650 Li-ion cells with a composite positive electrode by means of IC analysis. The degradation of NMC/G based Li-ion cells were studies in (6) under cycle aging for several depth-of-discharges whereas in (7), LTO cells were tested for 55 ^{o}C and the lifetime of three commercial cells was evaluated. In (8), Dubarry et al. investigated the capacity fade and the aging mechanisms of LFP cells for cycle aging and with discharge C-rates between C/25 to C/2.

Furthermore, different implementation techniques of the ICA have been proposed in the literature, starting from the most simple to directly differentiate the raw data of the capacity over the voltage to more advanced, by employing mathematical models and filters capable of providing more accurate and robust IC curves. Feng et al. (9) used a probability density function at the battery's terminals to generate the IC curve. Riviere et al. (10) built a health estimation model for LFP battery cells, using a butterworth filter for smoothing and identify the IC peaks. Weng et al. (11) analyzed the IC curves by comparing results from the simplest approach of direct fitting the charging curves, obtaining their functions and differentiate them, to a more advanced mathematical model with support vector regression to fit those charging curves. Lastly, Han et al. (2) divided the charging curves based on a specific voltage step, usually 5 mV, and by calculate the corresponding voltage samples in each step the IC peaks are plotted. The challenges of the ICA in general, are that it requires a constant current at low rates (C/25), and specifically for the last approach, a constant sample frequency in order to derive accurately the peaks is also required. The major advantage on the other hand, is that information about the degradation of the Li-ion battery cells can be obtained with a non-destructive approach. However, what is the suitability of this method for emerging battery technologies, such as Lithium-Sulfur (Li-S)?

Li-S batteries differ in many aspects from Li-ion batteries, as for example discussed by Propp et al. (12), a fact which in some cases prevents a straightforward transfer of the methods and approaches to be applied on them. Already at the method applicability, the first difference and challenge can be spotted by comparing the charging and discharging voltage profiles of the Li-ion and Li-S batteries, as illustrated in Fig 1. $LiFePO_4$/G (LFP) based cells have a flat voltage profile for a majority range of state-of-charge (SOC), except with end of charge and discharge. In contrary to that, $Li[NiCoMn]O_2$/G (NMC) voltage profile is continuously decreasing with decrease of the SOC. Thus, the strictly monotonous voltage curves are observed at the Li-ion batteries, while the typical Li-S voltage discharging curve has a 'dip' between the high- and low- voltage plateaus. Moreover, the Li-S charging curve can be monotonous or it can have a 'bump' (high internal resistance) at the beginning of the charging phase, according to the charging conditions and the previous cycling history. Furthermore, the two chemistries are driven by different mechanisms. The Li-ion batteries work based upon an intercalation mechanism, where the ions travel directly between the electrodes. On the other hand, the Li-S batteries are "solution chemistries", where reduction and oxidation reactions of several stages of polysulfide species take place during charging and discharging (13). Therefore, analyzing the incremental capacity (IC) curves should be done carefully by considering the aforementioned differences.

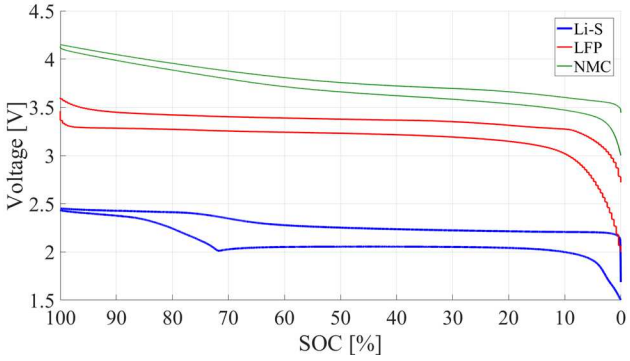

Figure 1. Comparison of charging and discharge voltage profiles of Lithium-Sulfur (Li-S), Lithium-iron-phosphate (LFP) and Lithium-nickel-manganese-cobalt-oxide (NMC) batteries.

Literature Review on ICA Applied to Li-S Batteries

ICA has not been widely applied to Li-S batteries. We have found only few sources which are present and discuss the IC curves. He et al. (14) used ICA for a graphical analysis of the pouch polymer battery with sulfur composite cathode and lithium foil anode in the size of 4×40×26 mm. The peaks in the IC curves are believed to stand for electrochemical reaction equilibriums, where the cathode material is reduced or oxidized. They detected two separate peaks during discharge at 2.10 V and 1.88 V, which implies that the cathode material reduction is happening in two steps in the composite. During the charging, two separate peaks were detected at 2.22 V and 2.36 V, which implies two charging plateaus related to two steps of the cathode material oxidation in the composite. The conclusion drawn is that the composite probably has two "active points" for lithium storage, which are connected to two voltage plateaus during charging and discharging. Ahn et al. (15) investigated coin cells with sulfur-MWCNT composite and precipitated sulfur as cathodes. They detected two peaks close to 2.45 V and 2.1 V during charge and discharge, which corresponds to the potential plateaus obtained from voltage profile during discharge. They are assigned to the formation of high-order (Li_2S_n, $4 \leq n \leq 8$), and low-order (Li_2S_n, $n < 4$) lithium polysulfides, respectively. Kim et al. (16) presented IC curves of a coin cell with HCS-S composite cathode to demonstrate its great electrochemical behavior, because of the full overlap of the peaks during the first and the second cycle. Moreover, this attribute, together with peak sharpness, should point out high reversibility and very fast electrode kinetics. Yersak et al. (17) applied the ICA to the all-solid-state Lithium metal batteries with FeS and S composite cathodes in order to understand and qualitatively determine parallel redox chemistries. A reduction peak at 2.2 V was characterized for S and it remained distinguishable also for the composite cathodes. In these previous works, where the ICA was applied to Li-S batteries, there is missing any note related to the unique character of the Li-S voltage profile and consequently to the specific forms, which are present in the dQ/dV plots.

In our work, we apply ICA to the pre-commercial 3.4 Ah Li-S pouch cells in order to evaluate its transferability to this battery chemistry. At first, the charging and discharging processes at different temperatures are investigated to observe the dQ/dV and also dV/dQ plots and their changes. It is followed by applying the ICA to the degrading cell by cycling to see if the ageing phenomena can be detected.

Experimental

Laboratory Tests

The performed experiments were conducted on a Digatron BTS 600 battery test station on the 3.4 Ah Li-S long-life type cells provided by OXIS Energy. The current of 3.4 A corresponds to 1 C-rate. The considered cut-off limits were 2.45 V or 11 hours for charging and 1.5 V for discharging. During the test, the cells were kept at the temperature controlled environment.

The test procedure for obtaining constant current charging and discharging curves consists of a pre-conditioning cycle (0.1 C-rate charging, 0.2 C-rate discharging) before every charging/discharging cycle at a specific rate. For charging, the currents of 0.1, 0.2 and 0.5 C-rate were used and for discharging, they were 0.1, 0.2, 0.5, 1.0, 1.5, 2.0, 2.5 and 3.0 C-rate. Three temperature levels of 15, 25 and 35 °C were investigated.

Filtering and Processing

The battery voltage was measured during charge/discharge cycle with a 0.2 mV resolution ADC with fixed-time sampling. A first derivative of the voltage is needed for the ICA analysis, however, calculating a derivative of a quantized data is a well-known challenge. The original measured data needs to be smoothed first before the derivative can be found.

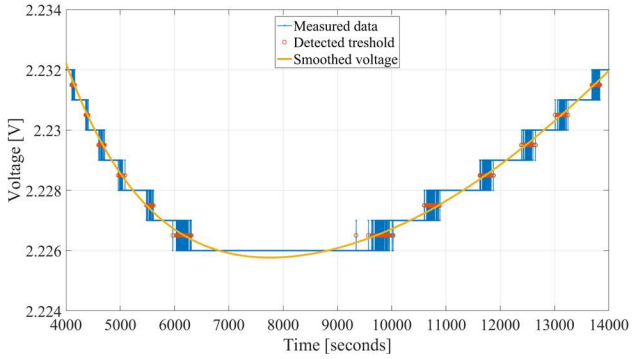

Figure 2. Measured voltage data, points extracted for smoothing and the final smoothed battery voltage.

In these tests, the battery voltage rises rapidly in the beginning of the charge cycle and then varies slowly during the last part of the cycle. Strongly varying signal dynamics poses challenges on finding a robust algorithm to smooth the data.

As can be seen in Fig. 2, the measured voltage data contained long stretches of time where the ADC converter would output a constant value. These portions of time have the highest quantization error. When the battery voltage crossed the threshold voltage of the ADC the quantization error is the smallest. The smoothing procedure creates a derived voltage data set that only included points when the ADC would change its output. These points are marked in Fig. 2 and are used further as a basis of creating a smoothed voltage waveform. A sliding window local fit is then utilized to find the smoothed voltage values.

Using the newly created points a 7-th order polynomial is fitted locally, around x_0, and the value of the polynomial at x_0 is taken as the smoothed value.

Results & Discussion

Charge Curves

For the state-of-health estimation, the charging curves have usually a greater significance than the discharging curves, because of the charging process is more likely to be performed by the constant current than the discharging in various battery applications. In Fig. 3, voltage charging curves for 0.1 C-rate for three temperature levels are shown. The charging curves for 15 and 25 °C have a monotonous trend, while the charging curve at 35 °C shows the kink in the beginning of charging. The monotonous curves can be easily represented in the dQ/dV plot, as it is also presented in Fig. 3, with the characteristic IC peaks. However, the non-monotonic curve shows discontinuity at the voltage level of the kink, which does not form an expected peak.

The obtained peaks at 25 °C are: a high peak at 2.205 V and a low peak at the high voltage spreading between 2.41 and 2.45 V. The low peak is actually composed of two peaks at 2.416 and 2.428 V. The voltage value of the peaks corresponds to the beginning of the low voltage plateau and to the high voltage plateau during charging, respectively. The observed characteristics are in good agreement with the presented IC curves in (15) and (16).

The remaining challenge is about the representing the voltage kink, existent for charging at 35 °C, in the terms of dQ/dV curves. The detail of the kink is shown in Fig. 4c). As the cell is charged, instead of the expected peak, there appears at first the curve with a sharp knee, which is followed by the curve with negative gradient and it ends by the positive decreasing curve followed by a rise to a higher voltage. This presentation prevents an intuitive graphical evaluation, even though it can be observed from Fig. 4a) that the characteristic features of the peak as the very steep rise and slower continuous descent is still present. However, when the data is plotted in an inverse manner as dV/dQ instead of dQ/dV, it provides a better representation of the voltage kink, which takes a form of the loop in the dV/dQ plot, as illustrated in Fig. 4d). No information is lost that way, but the curve features are getting another meaning and allow another intuitive analysis. The peaks in dV/dQ plot represent the voltage regions with higher gradient than previously the plateaus. The typical character of such dV/dQ curve is that it starts at very high values in the beginning of the charging and it decreases until the value close to the zero (for 0.1 C-rate it is approximately at 2.2 V, shown in Fig. 4b)), then either the loop representing the voltage kink starts, or it is followed directly by the slow rise of the peak, which later again decreases. The mathematical meaning stays same as it is demonstrated in Fig. 4e) and Fig. 4f). The dQ/dV peak at 2.427 V reaches the value of 34.22 Ah/V, while one can see in Fig. 4f) the valley at the same voltage with the value of 0.02922 V/Ah (1 / 34.22 = 0.02922).

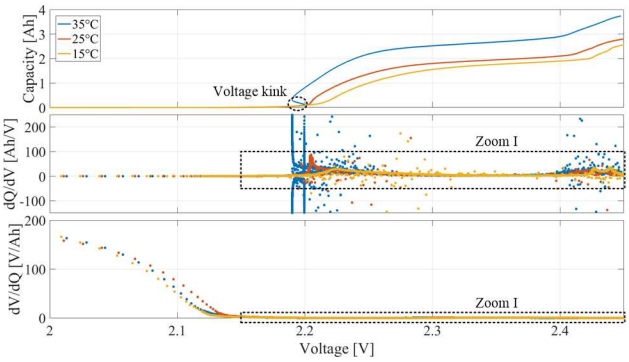

Figure 3. The charging curves for 0.1 C-rate at various temperature levels. The zoomed area is pictured in Fig. 4.

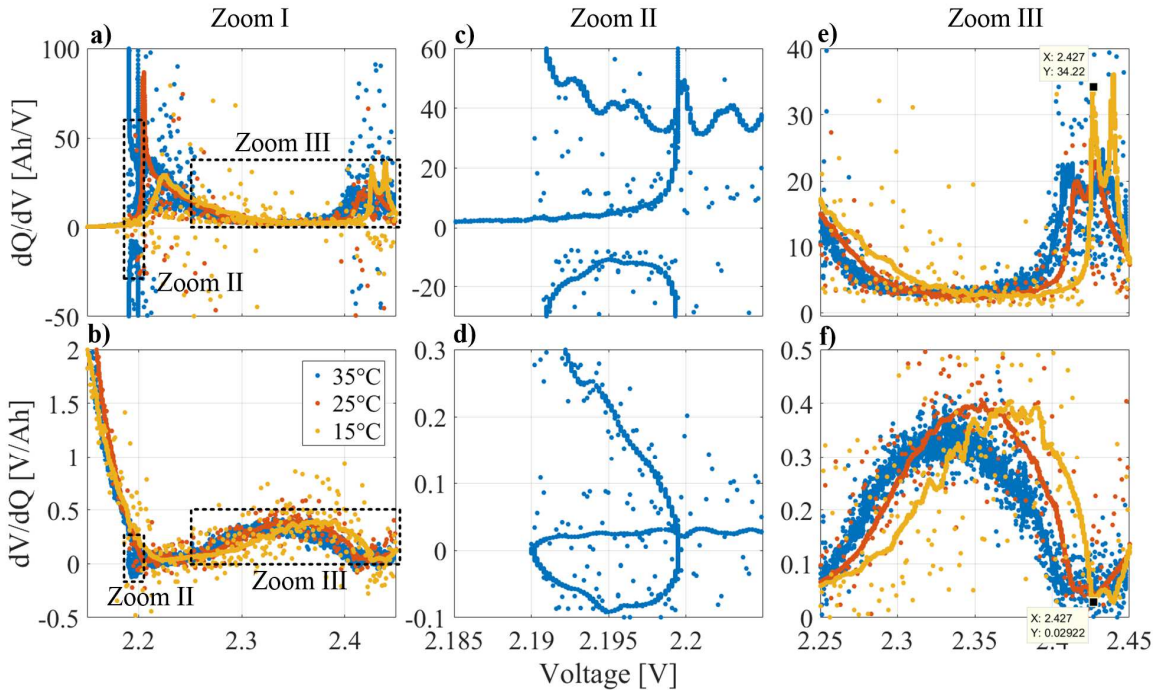

Figure 4. Detail plots for processed 0.1 C-rate charging curves at various temperature levels.

Discharge Curves

The voltage discharge curves have a different character than the charge curves for the Li-S batteries. However, at least for the small currents (0.1 C-rate), they result into fairly similar dQ/dV curves as shown in Fig. 5. There is a smaller peak at the high voltage plateau and there would be a high peak at the low voltage plateau, but due to the non-monotonic curve it results again into the discontinuity artefact. This discontinuity is represented again by a loop in the dV/dQ graph.

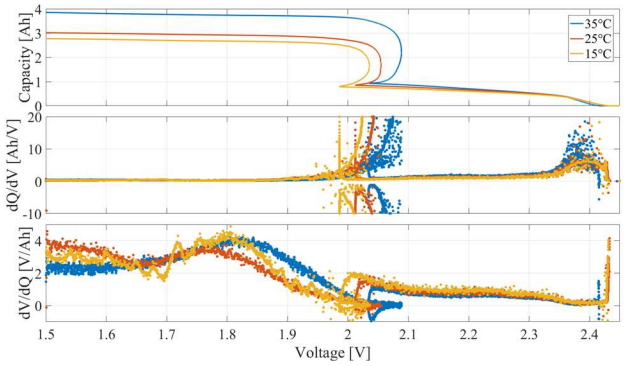

Figure 5. The discharging curves for 0.1 C-rate at various temperature levels.

Degradation Observations

In order to evaluate if ICA is a suitable method for the state-of-health estimation at the Li-S batteries, the Li-S cell was degraded by cycling at 30 °C by 0.1 C-rate charging until 2.45 V or 11 hours and by 0.2 C-rate until 1.5 V. A reference procedure test (RPT) was performed at the beginning of the life and then periodically every 20 cycles to capture the cells changing parameters such as the capacity or the impedance. The evaluation cycle, used for ICA, was performed at the same conditions as the cycling.

The visible sign of the degradation on the dQ/dV curves during discharging, presented in Fig. 6, is only at the peaks at the high voltage region, which are decreasing and moving towards higher voltage with an increasing degradation. The change with the clear trend at the dV/dQ curve is at the peaks appearing immediately after the loop. These peaks are growing and increasing in voltage. It seems that the degradation for these specific conditions is trackable through the dQ/dV and dV/dQ curves. However, the discharge curves do not provide many indicators.

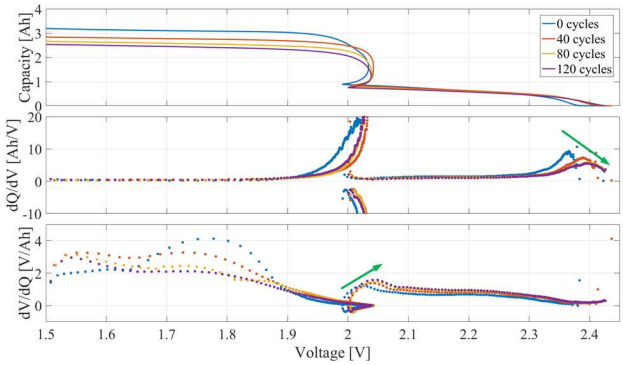

Figure 6. The evolution of the discharge curves for 0.2 C-rate during the aging cycling.

Contrary to the discharge curves, the charge curves provide several indicators of ageing, which makes them very suitable for the SOH estimation, even though the possibility of reversible degradation should be also considered. As it is noticeable from Fig. 7, the dQ/dV peaks at the high voltage plateau have a tendency to move to a higher voltage, which might be caused by the increased resistance, and to grow, which might be a sign of the growing effect of the polysulfide shuttle. At the low voltage plateau, there

was clearly one peak at the beginning of life, during ageing the growing kink appears, which results into discontinuity artefact on the dQ/dV curve. However, in this case its character is easier to observe. The curves at the positive plane forms still a sort of quasi-peak, which is decreasing and moving to the right, reflecting a loss of capacity and a resistance growth. As the voltage kink is becoming higher and steeper, the 'knee' at the negative plain is moving to the higher voltage and the top of the knee is getting closer to zero. These changes at the voltage kink area are also clearly visible on the dV/dQ plot, where the loop is increasing its volume and moving towards right. Another noticeable behavior is an increasing gradient in a transition from the low voltage plateau to the high voltage plateau, which is getting steeper during the ageing.

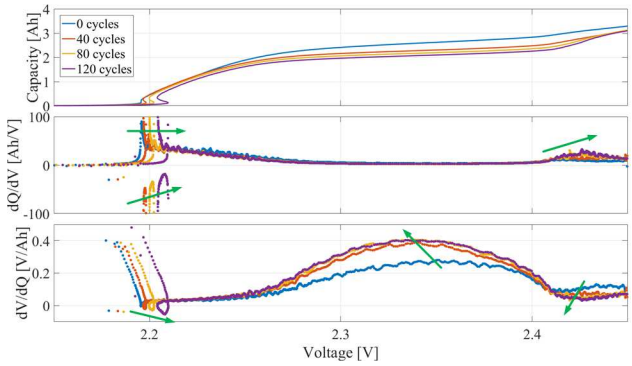

Figure 7. The evolution of the charging curves for 0.1 C-rate during the aging cycling.

Conclusions

The ICA technique was applied to charging and discharging voltage profiles of Li-S cells at various temperatures and unique behavior of the dQ/dV and the dV/dQ plots were detected. The 'classical' two peaks, at high- and low- voltage plateaus, are expected to be related to the formation of long and short polysulfide species, respectively. However, further relation of the curves to the specific mechanisms is missing. When applied to the cell undergoing degradation, the IC curves shown changing character, which reflects ageing phenomena and thus might allow for state-of-health estimation.

Acknowledgments

This work has been part of the ACEMU-project. The authors gratefully acknowledge the Danish Council for Strategic Research (1313-00004B) and EUDP (1440-0007) for providing financial support and would like to thank OXIS Energy for supplying the Lithium-Sulfur battery cells.

References

1. M. Dubarry, V. Svoboda, R. Hwu, and B. Yann Liaw, *Electrochem. Solid-State Lett.*, **9**, A454–A457 (2006).
2. X. Han, M. Ouyang, L. Lu, J. Li, Y. Zheng, and Z. Li, *J. Power Sources*, **251**, 38–54

(2014).
3. M. Kassem, J. Bernard, R. Revel, S. Pélissier, F. Duclaud, and C. Delacourt, *J. Power Sources*, **208**, 296–305 (2012).
4. M. Dubarry, B. Y. Liaw, M. S. Chen, S. S. Chyan, K. C. Han, W. T. Sie, and S. H. Wu, *J. Power Sources*, **196**, 3420–3425 (2011).
5. M. Dubarry, C. Truchot, M. Cugnet, B. Y. Liaw, K. Gering, S. Sazhin, D. Jamison, and C. Michelbacher, *J. Power Sources*, **196**, 10328–10335 (2011).
6. J. V. M. M. Berecibar, M. Dubarry, N. Omar, I. Villarreal, *Evs29*, 1–12 (2016).
7. X. Han, M. Ouyang, L. Lu, and J. Li, *Energies*, **7**, 4895–4909 (2014).
8. M. Dubarry and B. Y. Liaw, *J. Power Sources*, **194**, 541–549 (2009).
9. X. Feng, J. Li, M. Ouyang, L. Lu, J. Li, and X. He, *J. Power Sources*, **232**, 209–218 (2013).
10. E. Riviere, P. Venet, A. Sari, F. Meniere, Y. Bultel, U. Claude, B. Lyon, U. De Lyon, and V. Cedex, *Veh. Power Propuls. Conf. (VPPC), 2015 IEEE*, 1–6 (2015).
11. C. Weng, Y. Cui, J. Sun, and H. Peng, *J. Power Sources*, **235**, 36–44 (2013).
12. K. Propp, M. Marinescu, D. J. Auger, L. O'Neill, A. Fotouhi, K. Somasundaram, G. J. Offer, G. Minton, S. Longo, M. Wild, and V. Knap, *J. Power Sources*, **328**, 289–299 (2016).
13. M. Wild, L. O'Neill, T. Zhang, R. Purkayastha, G. Minton, M. Marinescu, and G. J. Offer, *Energy Environ. Sci.* (2015).
14. X. He, W. Pu, J. Ren, L. Wang, J. Wang, C. Jiang, and C. Wan, *Electrochim. Acta*, **52**, 7372–7376 (2007).
15. W. Ahn, K.-B. Kim, K.-N. Jung, K.-H. Shin, and C.-S. Jin, *J. Power Sources*, **202**, 394–399 (2012).
16. J. Kim, D. J. Lee, H. G. Jung, Y. K. Sun, J. Hassoun, and B. Scrosati, *Adv. Funct. Mater.*, **23**, 1076–1080 (2013).
17. T. a. Yersak, C. Stoldt, and S.-H. Lee, *J. Electrochem. Soc.*, **160**, A1009–A1015 (2013).